PHILOSOPHICAL TRANSACTIONS A

rsta.royalsocietypublishing.org

Review

Cite this article: Conforto E, Guillot I, Feaugas X. 2017 Solute hydrogen and hydride phase implications on the plasticity of zirconium and titanium alloys: a review and some recent advances. *Phil. Trans. R. Soc. A* **375**: 20160417.
http://dx.doi.org/10.1098/rsta.2016.0417

Accepted: 17 February 2017

One contribution of 24 to a discussion meeting issue 'The challenges of hydrogen and metals'.

Subject Areas:
materials science, crystallography, electron microscopy

Keywords:
titanium, zirconium, visco-plasticity, solute hydrogen, hydrides, strain hardening

Author for correspondence:
X. Feaugas
e-mail: xfeaugas@univ-lr.fr

Solute hydrogen and hydride phase implications on the plasticity of zirconium and titanium alloys: a review and some recent advances

E. Conforto[1], I. Guillot[2] and X. Feaugas[1]

[1]LaSIE UMR CNRS 7356, University of La Rochelle, Av. Michel Crépeau, 17042 La Rochelle, France
[2]ICMPE (UMR 7182), CNRS, UPEC, Paris East University (UPE), 94320 Thiais, France

XF, 0000-0003-4954-0887

In this contribution, we propose a review of the possible implications of hydrogen on mechanical behaviour of Zr and Ti alloys with emphasis on the mechanisms of plasticity and strain hardening. Recent advances on the impact of oxygen and hydrogen on the activation volume show that oxygen content hinders creep but hydrogen partially screens this effect. Both aspects are discussed in terms of a locking–unlocking model of the screw dislocation mobility in prismatic slip. Additionally, possible extension of this behaviour is suggested for the $\langle c + a \rangle$ pyramidal slip. The low hydrogen solubility in both Zr and Ti leads in many cases to hydride precipitation. The nature of these phases depends on the hydrogen content and can show crystallographic orientation relationships with the hexagonal compact structure of the alloys. Some advances on the thermal stability of these phases are illustrated and discussed in relation with the deepening of the misfit dislocations. Under tensile loading, we showed that hydrides enhance the hardening process in relation with internal stress due to strain incompatibilities between the Zr and Ti matrix and hydride phases. Different plastic yielding processes of hydrides were identified, which progressively reduce these strain incompatibilities.

This article is part of the themed issue 'The challenges of hydrogen and metals'.

THE ROYAL SOCIETY PUBLISHING

1. Introduction

By virtue of the conditions necessary during processing and application environments, hydrogen is intimately associated with titanium and zirconium alloys. Hydrogen can favour the refinement of some microstructures of titanium alloys [1], and thus offer better biocompatibility [2]; however, this can also lead to possible embrittlement shown in several industrial applications [3]. These cases of embrittlement are strongly linked to the interaction of the hydrogen with the crystal structure and the specific mechanisms of plasticity exhibited by these alloys. Titanium and zirconium alloys present a significant number of deformation modes (five slip systems and four deformation twin modes) [4,5], which should confer high ductility. However, this theoretical ductility is strongly mitigated by the deformation modes having very different critical resolved shear stresses (CRSS) [5–7]. In the case of Ti-α and Zr-α, the prismatic slip $a/2\langle 1\bar{2}10\rangle\{10\bar{1}0\}$ ($\langle a\rangle$ − P) is currently recognized as the easiest slip mode. $\langle a\rangle$ dislocations with Burgers vector $a/2\langle 1\bar{2}10\rangle$ may glide also in the basal plane (0001) or in a first-order pyramidal plane $\{10\bar{1}1\}$, which are defined as secondary slip systems. Cross-slip of $\langle a\rangle$ dislocations in first-order pyramidal planes $\{10\bar{1}1\}$ is also observed. For all these slips systems, $\langle a\rangle$ dislocations cannot accommodate strain along the $\langle c\rangle$ axis of the hexagonal close-packed lattice; consequently additional deformation modes are needed, which correspond to twin modes or $\langle c+a\rangle$ ($a/3\langle 11\bar{2}3\rangle$) Burgers vector gliding either in the $\{10\bar{1}1\}$ first-order pyramidal plane (π_1) or in the $\{10\bar{1}2\}$ second-order pyramidal plane (π_2). In numerous cases, ease of Ti-α and Zr-α to deform plastically in selected crystallographic planes depends on the mobility of the screw dislocation in relation with the core structure of its dislocations. The involvement of the oxygen and the hydrogen atoms and their interactions with the dislocation core are fundamental to solve the thermodynamic processes, which would explain the viscoplastic behaviour and the anisotropy in Ti-α and Zr-α alloys [5–7]. We shall go over this last point in the present paper referencing recent experimental work. As long as Ti-α and Zr-α accept hydrogen in solid solution, it is randomly distributed to energetically favourable tetrahedral sites [8,9]. Knowing the limits of solubility of hydrogen in the material is fundamental to understanding the role of hydrogen in the material's mechanical properties. The Ti–H and Zr–H equilibrium phase diagrams show that H solubility is very low at ambient temperature, and therefore will quickly form hydride phases ZrHx and TiHx [10]. The nature of the precipitate phases depends on the hydrogen content and the temperature stability will define the crystallographic relationships existing between the hydride and the matrix (α-phase), and we shall discuss these with reference to our experimental work [11]. At ambient temperature, the hydrogen atoms are mostly found in the form of hydrides; consequently, it seems important to improve the understanding and clarify the dislocation/hydride interactions and their consequences on the strain hardening of Ti-α and Zr-α alloys. Therefore, the present review focuses on the impact of hydrogen atoms on the plasticity of the Ti and Zr alloys; some fundamental properties will be summarized and discussed:

— The effect of solute hydrogen atoms on dislocation mobility in the different slip systems.
— The nature of hydrides, their crystallographic relationship with α-phase, and their thermal stability.
— The interaction between hydrides and deformation mechanisms and their implications on strain hardening.

2. The effect of hydrogen on the accommodation of plastic deformation

The plastic strain accommodation in Ti and Zr alloys is strongly affected by solute content, especially oxygen. Therefore, to understand the impact of hydrogen solutes on plastic behaviour, we must also take into account the interaction of oxygen solutes. Oxygen solutes generally lead to significant hardening and modify the strain rate sensibility of the stress in relation to a possible modification of the dislocation core structure.

Numerous experimental observations demonstrate the non-planar character of the dislocation core of the type $\langle a \rangle$ dislocations (see [12–14] for a review). In particular, transmission electron microscopy (TEM) *post-mortem* observations ($T < 673$ K) show long screw dislocations. Furthermore, during *in situ* TEM tensile tests, the works of Naka *et al.* [15] and of Farenc *et al.* [16] demonstrate a large difference in dislocation mobility between the screw and edge dislocations, the latter presenting a planar structure [17]. The nature of the several planes of core spreading of the $\langle a \rangle$ screw dislocations remains a subject of controversy. There is a wide consensus on the core spreading on the prismatic plane and the possibility of having some secondary spreading in basal and first pyramidal planes. Indeed, while Naka *et al.* [15] propose the first pyramidal planes as a secondary spreading possibility, the main atomistic works relate a screw dislocation core with a basal spreading plane [9,18–20]. More recently, Clouet *et al.* revisit these calculations and demonstrate that the spreading in prismatic and first pyramidal planes are stable configurations, while the configuration in the basal plane is unstable for pure Ti and Zr metals [21,22]. Therefore, screw dislocations have been shown to dissociate into more than one plane and undergo non-planar dissociation, and are likely the reason for the high level of frictional stress and high dependence of yield stress on temperature exhibited in these alloys. Both of these properties strongly depend on the solute content and especially the oxygen content [5,12]: the strain rate sensitivity of stress and the critical resolved shear stress of prismatic slip increases very effectively as a function of oxygen content [5,6,14]. Clouet *et al.* have commented on this hardening effect using recent atomistic calculations [22]. The possible source of hardening suggested is associated with a strong repulsion of oxygen and a modification of the dislocation core structure which promotes cross-slip on the π_1-plane. The $\langle a \rangle$ dislocations can also move on two planes: the basal plane B and the first pyramidal planes π_1, which are recognized as secondary slip systems. The basal slip system is generally observed only for well geometrically oriented crystals and large plastic strain [5–7,12,16,23–33]. The CRSS of basal slip and the strain rate sensitivity of stress are higher than the ones reported for prismatic slip for a large range of temperatures and oxygen content [5,6,12]. However, it should be noted that these differences decrease as a function of temperature and oxygen concentration in Ti-α and Zr-α [5,6,34] and aluminium concentration in Ti-α [29,30].

The first pyramidal plane π_1 is often described as the cross-slip plane of $\langle a \rangle$ screw dislocations [12–16,24]. On the other hand, the basal plane has also been observed as a cross-slip plane in high purity titanium alloy [16]. Therefore, we may infer that the active cross-slip plane depends on the oxygen content (basal for pure metals and π_1 in the presence of oxygen). Consequently, the understanding of the effect of oxygen solute content on dislocation core behaviour needs to be improved in future works. The $\langle a \rangle$ π_1 is not only a cross-slip system but also a secondary slip system as identified by some authors [12,31,33]. Its CRSS is higher than the one of the prismatic slip plane and the difference seems to decrease with the addition of oxygen [6,16].

The deformation along the $\langle c \rangle$ axis is associated with the two secondary deformation modes, which are the twinning and the slip with a $\langle c + a \rangle$ Burgers vector. These can be present simultaneously in a grain [12]. Nevertheless, the presence of oxygen and/or aluminium is unfavourable for the twinning process and favours the pyramidal slips (π_1 and π_2) of $\langle c + a \rangle$ dislocations. The $\langle c + a \rangle$ slip plane depends on dislocation character (screw or edge) and the stress loading direction. Atomistic calculations suggest that the $\langle c + a \rangle$ dislocations glide in the $\{10\bar{1}1\}$ plane for a negative shear stress (tensile loading along [0001]) and glide in the $\{11\bar{2}2\}$ plane for a positive shear stress (compression along [0001]) [35–37]. Numerous TEM observations in various titanium and zirconium alloys confirmed this feature [12,38–40]. The CRSS, τ_c and the stress sensitivity to the plastic strain rate are much higher than those reported for the other slip systems. Moreover, τ_c depends on the stress direction (lower in tension than in compression). The $\langle c + a \rangle$ core structure has not been clearly investigated; consequently, the nature of the spreading planes remains unknown.

In spite of the possible activation of secondary slip, prismatic slip generally accommodates most of the plastic deformation in the early stages of deformation for the orientations favourable to the mobility of $\langle a \rangle$ dislocations. In particular, the stress sensitivity to the plastic strain rate is

associated with the mobility of the $\langle a \rangle$ screw dislocations in the prismatic planes. *In situ* TEM tensile tests on Ti-α single crystals show that, at low temperature ($T \leq 473$ K), the jerky movement of the screw dislocations accommodates the plastic deformation, which indicates the occurrence of a locking–unlocking mechanism [16,41]. Indeed, the mobility of the edge dislocations is much greater than that of the screw ones at low temperatures. Consequently, the screw dislocations are the only ones that control the plastic deformation. Precise analysis of *in situ* TEM experiments, paying attention to the changes in the activation volume as a function of temperature, shows that there exists a transition (for a temperature close to 300 K) between a mechanism of constriction of the dislocation core described by a formalism developed by Friedel–Escaig, and a double-kink mechanism which is associated with the Peierls model [42]. The constriction of the secondary spread planes of the sessile configuration onto glissile configuration in the prismatic plane is characterized by the recombination energy ΔE, associated with the Friedel–Escaig mechanism. This recombination energy is an increasing function of oxygen concentration [41,43]. In other words, oxygen affects the core structure of the screw $\langle a \rangle$ dislocations and directly impacts the physical (lattice) parameter, which describe the dislocation mobility.

The jump distance between two sessile configurations h_s, directly deduced to the Peierls model, is at each condition greater than the distance between two adjacent Peierls valleys [13,43]. Additionally, the jump distance is a decreasing function of the oxygen content [13,43]. Oxygen therefore seems to be at the origin of a jump distance. However, many points remain unclear; in particular, the nature of the interaction between oxygen atoms and dislocations is unknown. Furthermore, the dynamic interactions between dislocations and oxygen encountered around 623 K in the alloys of titanium and zirconium are still poorly understood.

Uniaxial tensile loading favours the activation of $\langle c + a \rangle$ slip (requiring the accommodation of strain along the $\langle c \rangle$ axis); this $\langle c + a \rangle$ π_1 activation is observed in the majority of plastically deformed grains in polycrystalline material [13,14]. This property leads to larger strain rate sensitivity in relation to a lower activation volume for these slip systems [6,13,14]. It seems that for this stress configuration, a rotation of the $\langle c \rangle$ axes takes place rapidly in the early stages of the deformation, which promotes the activation of prismatic slip. Thus, at higher plastic strain, we observe similar strain hardening and strain rate sensitivity [13,14]. As in the case of prismatic slip, oxygen content reduces the activation volume of the $\langle c + a \rangle$ slip suggesting similar mechanisms for these dislocations in terms of mobility to those proposed for the mobility of screws $\langle a \rangle$ [14]. This last point deserves to be confirmed by *in situ* TEM observations.

Owing to its low solubility and high mobility, the effects of hydrogen in solution on the mechanical behaviour of titanium and zirconium alloys have been less studied. Nevertheless, some points are now well established. Tensile tests performed on zirconium alloys in the range of 250–400°C highlight the fact that the hydrogen content leads to a stress softening that depends strongly on the oxygen content (figure 1). Additionally, an increase in creep velocities has also been observed [14,44,45]. Using the relaxation tests for the same alloys, it was found that hydrogen increases the activation volume for moderate oxygen content (0.31% in equivalent oxygen content O_{eq}). On the other hand, no significant effect was observed for larger oxygen content (table 1) [14]. This last point appears to be confirmed by results obtained in zircaloy-4 (0.8 at% in O_{eq}), where the hydrogen content has negligible effect on the activation volume [44]. All these results are unaffected by different stress orientations despite the crystallographic texture [47]. Thus, the role of hydrogen is similar on $\langle a \rangle$ and $\langle c + a \rangle$ slip systems (table 1).

All the features just discussed seem to be associated directly with the presence of oxygen and its effect on screw dislocation mobility; therefore, the common explanation given for the impact of hydrogen in terms of elastic shielding effect cannot be possible in Ti-α and Zr-α alloys [48–50]. Despite this, *in situ* TEM observations under hydrogen pressure highlight an increase in screw dislocation mobility with hydrogen content in Ti-α [51]. Using *ab initio* calculations based on density functional theory, Domain *et al.* have studied the interaction of hydrogen with stacking faults in the Zr–H solid solution. Hydrogen seems to reduce stacking fault energies, which favours the spreading of the dislocation core in the prismatic plane and consequently hinders cross-slip [46]. In fact, there are no experimental results to confirm these observations and the interactions

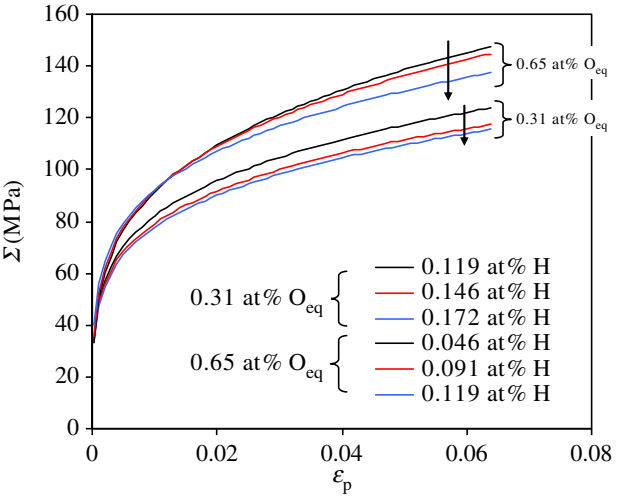

Figure 1. Consequence of hydrogen and oxygen content on tensile stress–strain curve of polycrystalline zirconium alloys at 573 K ($\dot{\varepsilon} = 2 \times 10^{-4}$ s^{-1}). (Online version in colour.)

Table 1. Impact of hydrogen and oxygen content on the activation volume V/b^3 of the prismatic slip $\langle a \rangle$P and the pyramidal slip $\langle c + a \rangle \pi_1$ (tensile and relaxation tests at a temperature of 300°C for zirconium alloys) [43].

	0.31 at% O_{eq}		0.65 at% O_{eq}	
at% H	$\langle a \rangle$P	$\langle c + a \rangle \pi_1$	$\langle a \rangle$P	$\langle c + a \rangle \pi_1$
0.046	—	—	90	30
0.119	128	44	—	—
0.540	147	60	88	34

between hydrogen and oxygen are not considered in these calculations. On the other hand, atomic simulations demonstrate a repulsive interaction between oxygen and hydrogen at a very short distance in the atomic network of Zr-α [46]. Hydrogen solutes, located on the tetrahedral sites, in the vicinity of a screw dislocation are therefore likely to decrease the number of octahedral sites available for oxygen by a simple repulsive effect. This analysis is in agreement with the increase of the activation volume as a function of the hydrogen content observed at 300°C (table 1). Indeed, at this temperature the evolution of the activation volume is associated with an increase in the jump distance of a screw dislocation between two sessile configurations. The decrease in the number of available octahedral sites for oxygen in the presence of hydrogen thus seems to lead to an increase in the jump distance and consequently to a decrease in the strain rate sensitivity. This last point deserves to be confirmed by TEM *in situ* tensile tests performed under partial pressure of controlled hydrogen. If all of this work is very promising, it should not be forgotten that oxygen and hydrogen are mobile in the temperature regime considered (250–400°C). Consequently, the jump distance h can be considered as only one average value at a given time.

3. Hydride phases and crystallographic orientation relationships

The spontaneous nucleation and growth of hydride precipitates observed in materials such as titanium, zirconium and their alloys occurs due to the very fast hydrogen diffusion and the low solubility threshold. The volume expansion generated by the hydride precipitation (around 15%) induces high internal stresses [14,52] at the origin of a decreased toughness [53]. Three different hydride phases can then precipitate, γ, δ and ε, whose structure and morphology depend on

Table 2. Characteristics of the various hydride phases in α-Ti and α-Zr [10,54–71].

hydride	metal	composition	crystallographic parameters (nm)	orientation relationship	volume dilatation
γ (FCT)	α-Ti	TiH	$a = 0.420$	OR1	12.5–14%
			$c = 0.470$	OR2	
	α-Zr	ZrH	$a = 0.462$	OR1	12.3–15.7%
			$c = 0.489$	OR2	
δ (FCC)	α-Ti	TiH_x	$a = 0.440$	OR1	21–29%
		$1.5 < x < 1.99$		OR3	
				OR4	
	α-Zr	ZrH_x	$a = 0.478$	OR2	16.3–17.2%
		$1.5 < x < 1.9$		OR1[a], OR3[a]	
ε (FCT)	α-Ti	TiH_x	$a = 0.447$	OR1	3–14.1%
	α-Ti	$1.8 < x \leq 2$	$c = 0.440$	OR3	
	α-Zr	ZrH_x	$a = 0.495$	—	—
		$1.71 < x \leq 2$	$c = 0.446$		

[a]Recent results reported in [11,72].

the hydrogen content (table 2) [10,54–71]. The metastable γ-TiH phase, which precipitates in H-poor Ti, shows long and thin lamellae of face-centred tetragonal (FCT) structure with $c/a > 1$. Hydrogen atoms occupy tetrahedral sites of (110) planes. The stable face-centred cubic (FCC) δ-phase of CaF_2 structure type develops at intermediate H content with a random occupation of sites. In the literature, another FCT phase is reported (the ε one) for which $c/a < 1$. In some situation, the three phases can exist simultaneously.

Various factors influence the hydride precipitation (composition, texture, work-hardening, etc.). On the one hand, intermediate/high hydrogen contents and slow cooling favour δ-hydride precipitation, increasing the proportion represented by this phase in the ensemble of hydride precipitates. On the other hand, after fast cooling, the γ-hydride is often observed. The δ-hydride precipitation is favoured under traction or shear stress, meanwhile γ-hydride formation is observed in the absence of stress [54,72]. Hydrides tend to precipitate in a plane perpendicular to the tensile direction [55,73,74]. The content of the alloy elements influences the hydride nature (γ or δ) [73]. In particular, zirconium alloys with oxygen concentrations higher than 1000 ppm favour the precipitation of δ-hydride. The precipitation sequence for hydrides of different natures can be different depending on several factors: the total and local hydrogen content, and the crystallographic orientation of the matrix. In general, the stable δ-hydride is directly formed at the Ti interface: TiH_x/Ti for favourable crystallographic orientations or through the formation of the intermediate, γ-TiH phase. The transformation from γ-TiH to δ-TiH_x occurs without changes in the orientation relationships with the α-Ti matrix [56].

We observe that decreasing the hydrogen content in the δ-phase associated with the hydrogen diffusion can lead to the inverse transformation: $\delta - \gamma$ [75]. This result was confirmed for global and local approaches in recent works on Zr alloys [11]. The γ-phase forms from the α-phase via a shearing of the hexagonal lattice simultaneously to hydrogen atom diffusion [76]. The $\delta - \gamma$ transformation seems to follow a similar mechanism [75]. The formation of the δ-phase from the α-phase follows a transformation of a near-martensitic type [77].

The crystallographic coherence between the hexagonal substrate and the hydride precipitates is fairly high. In previous works, TEM bright-field (BF) images and selected area electron diffraction (SAED) patterns allowed the identification of four particular epitaxial orientation relationships (ORs) [56,64–66,78,79] between the CPH matrix and FCT and FCC hydrides. The

ORs observed for the three hydride phases in α-Ti and α-Zr are listed in table 2. Recently, OR1 [72] and OR3 [11] were also observed in δ-hydrides/α-Zr. Investigations on the existence of other ORs between zirconium hydrides and the matrix are in progress. The parallel planes, the parallel zone axes between the two phases for each OR as well as those at the interface are:

OR1 : $(0001)//(001)$, $[1\bar{2}10]//[110]$, interface plane $(10\bar{1}0)//(2\bar{2}0)$
OR2 : $(0001)//(1\bar{1}1)$ (angle of 4°), $[1\bar{2}10]//[110]$, interface plane $(10\bar{1}3)//(2\bar{2}0)$
OR3 : $(10\bar{1}0)//(\bar{1}11)$, $[1\bar{2}10]//[110]$, interface plane $(0001)//(2\bar{2}4)$
OR4 : $(\bar{1}011)//(001)$, $[1\bar{2}10]//[110]$, interface plane $(10\bar{1}1)//(\bar{1}11)$

Dislocations are necessary to accommodate the misfit between FCT and FCC hydrides and the hexagonal matrix [61]. Carpenter *et al.* propose that the large shear strains associated with the precipitation mechanism may play an important role in the preferential orientation of hydrides under stress [62]. More recently, other authors have quantified the density of dislocations in zirconium hydride, which seems to be higher than those in the zirconium matrix [80,81].

Thermodynamic parameters play a crucial role in the dissolution/precipitation mechanisms of hydride phases in zirconium alloys. Thermodynamic investigations on a global scale [11], consisting of thermal cycling of samples with different hydrogen contents using differential scanning calorimetry (DSC) for a large number of cycles, show that both dissolution and re-precipitation temperatures increase with the number of cycles. It was observed that the dissolution temperature is higher than that of precipitation and is independent of the hydrogen content in the range investigated. This difference in temperature can be discussed in terms of energy. In fact, many authors have been measuring the activation energy, the entropy and enthalpy for these processes in different zirconium alloys [82–85] by performing thermal-cycling measurements with a global approach (over a large density of hydrides). According to these authors, the dissolution enthalpy is slightly higher than that of precipitation for many different zirconium alloys. However, the same kind of experiment performed in zircaloy-4 containing gamma-hydrides shows a larger difference in enthalpy (28 kJ mol^{-1}) [72] between dissolution and precipitation, where the dissolution enthalpy is higher than the precipitation one. Mathematically, the difference between both enthalpies is only dependent on the stored elastic and plastic energies. The experimental difference observed can thus be attributed to misfit dislocations.

TEM *in situ* measurements in the same kind of sample confirm this hypothesis (figure 2). In fact, misfit dislocations were observed at the γ-ZrH/Zr interface at 300 K before heating (figure 2*b*). In the same figure, the depinning of a misfit dislocation is observed at 700 K when the dissolution is completed. This means that part of the hydrogen atoms from the dissolved precipitate are driven away from the precipitation region and are no more available to re-precipitate [86]. In terms of dissolution temperature range, slight differences may be observed between an *in situ* heating experiment (where a single precipitate is observed at a local approach) and DSC cycling (a large number of precipitates involved in a global approach). By TEM, the beginning of the dissolution process is observed at temperatures lower (figure 2*a*) than that indicated by the heating rate curve in figure 2*c* at a global scale. However, images show that the hydride main volume dissolves in the temperature range of figure 2*c*. Similar results were obtained by *in situ* TEM performed in zircaloy-4 samples richer in H, where only FCC δ-hydride precipitates were observed. This indicates a good agreement between global measurements (DSC) and *in situ* TEM observations at a local scale.

The decrease in concentration of hydrogen atoms available to precipitate can explain the difference in energy between dissolution and precipitation after a thermal cycling for a global approach. Moreover, the accumulated effect of multiple misfit dislocations depinning after a large number of cycles can lead to the precipitation of hydrogen-poor hydride phases. In fact, the simultaneous presence of the initial hydrogen-rich phase (the FCC δ-hydride) and a hydrogen-poor phase (the γ-FCT) was observed at the hydride–substrate interface after cycling, as shown in figure 3. The re-precipitation of the δ-hydride after 20 thermal cycles is still highly coherent

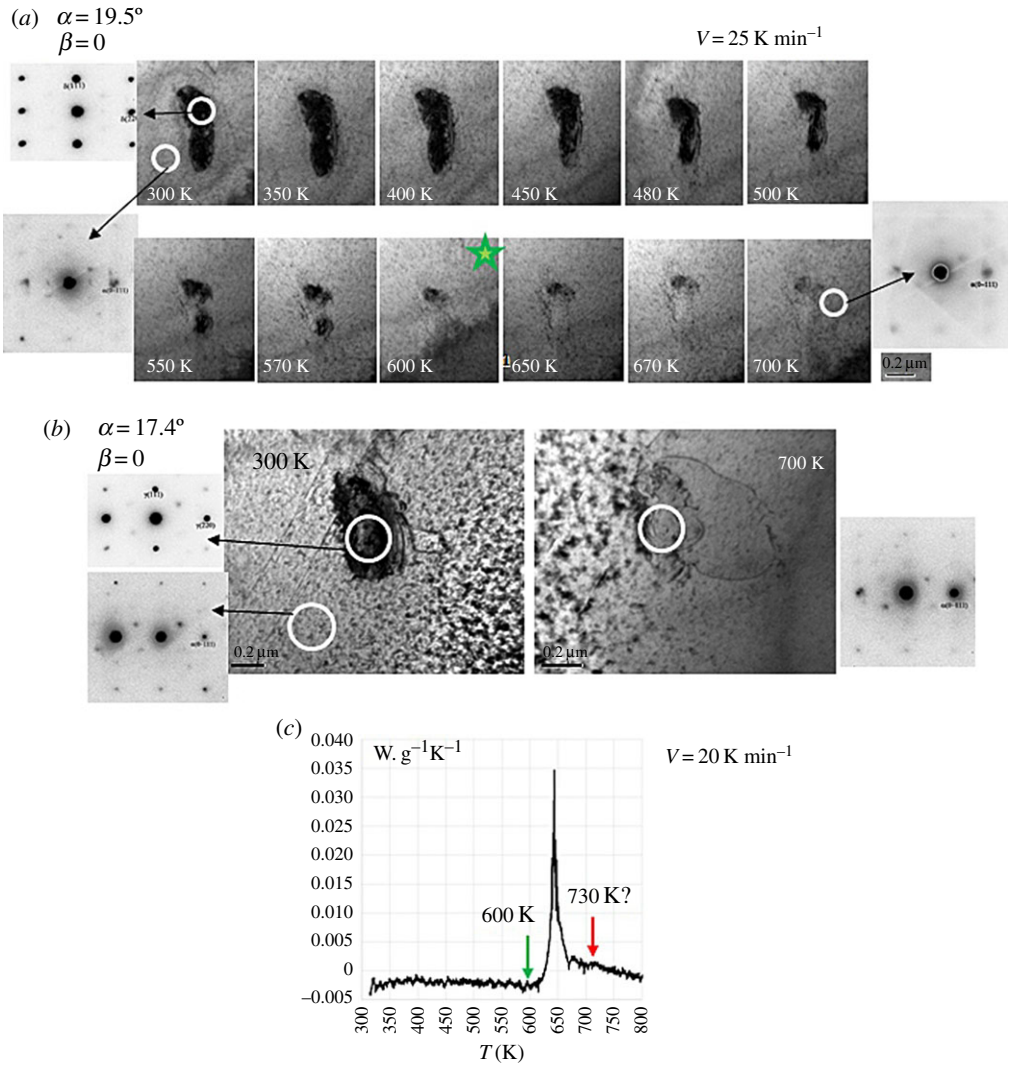

Figure 2. (*a*) *In situ* TEM images of FCT γ-hydride dissolution (300 K $< T <$ 700 K) in zircaloy-4 sample with 112 wppm in H showing the beginning of the process around 430 K, observable at local scale. The main dissolution is observed between 600 and 730 K, in good agreement with the heating rate as a function of the temperature at a global scale by DSC in (*c*). (*b*) Depinning of a misfit dislocation allowing hydrogen atoms to diffuse far from the re-precipitation region. (Online version in colour.)

with respect to the substrate (orientation close to an OR3 in this case) and the (220) planes of the γ-FCT phase are parallel to those of the γ-FCC (figure 3*c*,*d*).

4. Some interactions between hydrides and deformation modes and their implications on strain hardening

Numerous works describe hydrides as a brittle phase based on the significant reduction in the ductility of the hydrided titanium and zirconium alloys, the hydrides being considered fragile for temperatures below 150°C [77,87,88]. By contrast, above 150°C titanium and zirconium hydrides are most often found to have a ductile behaviour [89–91]. The study of the behaviour of solid hydrides, supplemented by nanoindentation tests, demonstrated the ductile nature of the hydrides [91]. However, the hardness and the yield stress at room temperature are very

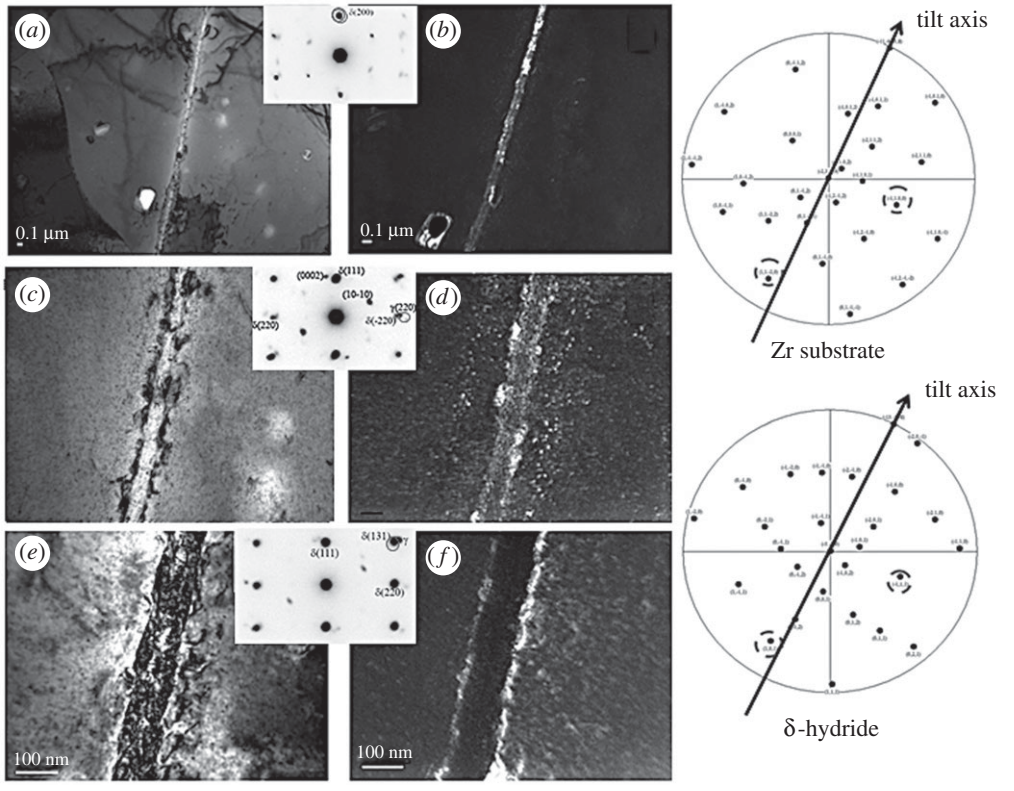

Figure 3. TEM images and SAED patterns showing the simultaneous presence of δ- and γ-hydrides in a zircaloy-4 sample with 356 wppm in H after 20 thermal cycles by DSC. Before cycling only the presence of δ-hydride precipitates was detected in this sample.

sensitive to the hydrogen content and therefore to the nature of hydrides both for titanium and for zirconium and its alloys. Most authors [92–99] show that titanium or zirconium hydrides (γ, δ or ε) have a higher Young's modulus, hardness and yield strength than those of pure metal but decrease with increasing hydrogen content. Only Setoyama *et al.* [100] observe a decrease in Young's modulus and Vickers hardness of δ-hydrides TiH_{2-x} compared to pure titanium.

Owing to the indentation size effect (ISE), the hardness measurements are scattered. Rico *et al.* [97] obtain an average value of 1.75 GPa for the zirconium alloy (Zirlo) and 2 GPa for the δ-zirconium hydrides, whereas the values of Yamanaka *et al.* [94], obtained by microhardness, are between 2.4 and 2.6 GPa for the δ-hydride bulk sample. Because the large penetration depths due to microhardness tend to eliminate the ISE, the microhardness measurements of Yamanaka *et al.* [94] are in good agreement with the true hardness obtained by nanoindentation with the Nix & Gao model [98]. On the other hand, Xu & Shi [95] measured by nanoindentation an average hardness of the zirconium matrix of 4.8 GPa and ε-hydrides of 3.3 GPa which is too high because of ISE at the low penetration depths. The same problem is found with the results of Kuroda *et al.* [96] (4 GPa) and those of Oono *et al.* [99] (3–4 GPa) for δ-zirconium hydride. It can simply be concluded that the δ-hydrides are harder than the ε-hydrides and harder than the zirconium matrix. The yield stress is also very sensitive to the nature of the hydride. For example, at ambient temperature for the Zr–2.5Nb alloy, the mean yield stress of the γ-, δ- and ε-hydrides is $\sigma_y(\gamma) = 540$ MPa, $\sigma_y(\delta) = 680$ MPa and $\sigma_y(\varepsilon) = 200$ MPa, respectively [91]. These high elasticity limits make hydrides a 'hard' phase for inclusion in a more ductile α-phase matrix. Thus at 25°C the ε-hydride exhibits good ductility and a high work hardening ($\theta = 15$ GPa), the γ-hydride is

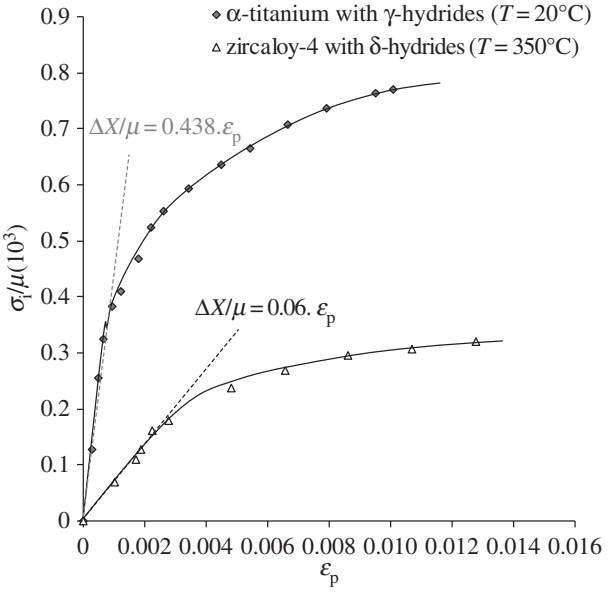

Figure 4. Tensile tests: evolution of the internal stress increment associated with the presence of hydrides γ and δ, respectively, for α-titanium at 20°C ($\Gamma = 0.9$, $\mu = 40$ GPa, $D = 1.63$, $f_v = 12.5\%$) [52] and zircaloy-4 at 350°C ($\Gamma = 0.85$, $\mu = 26$ GPa, $D = 1$, $f_v = 3.5\%$) [44].

less ductile and hardens slightly ($\theta = 1.25$ GPa) and finally the δ-hydride has a very low ductility and a high work hardening ($\theta = 10$ GPa) [91].

The behaviour of hydrided titanium and zirconium alloys is therefore to be compared with the general framework of alloys reinforced by a second phase. It has been shown by load–unload tests that the presence of hydrides induces long-distance internal stresses σ_i, which harden α-titanium [52] and zircaloy-4 [44]. The internal stress increment ($\sigma_i = \Delta X$) allocated to the hydrides first evolves linearly as a function of the plastic deformation (ε_p) and then appears to stabilize (figure 4). This linear behaviour of ΔX as a function of ε_p observed during the first stage of deformation corresponds to the hardening of a material containing a second phase that deforms elastically. The slope of this linear domain can then be estimated by an Eshelby inclusion approach [101]. For lattice precipitates, ΔX is given by the following equation:

$$\Delta X = X(\mathrm{MH}_{2-x}) - X(\mathrm{M}) = 2\Gamma D \mu f_v \varepsilon_p, \tag{4.1}$$

where Γ is a dimensionless parameter taking into account the shape of hard phase particles (hydrides), μ the shear modulus of the matrix, D the modulus correction factor in relation to elastic inhomogeneity, f_v the volume fraction of the hard phase and M the alloy, pure titanium or zircaloy-4. The theoretical slopes obtained with the expression above are close to the experimental one (figure 4). The hydrides can therefore be considered as hard inclusions, deforming only elastically up to a material- and temperature-dependent threshold ($\varepsilon_p = 0.16\%$ for α-titanium at 25°C and $\varepsilon_p = 0.25\%$ for zircaloy-4 at 350°C). Beyond this threshold, the loss of linearity corresponds to a relaxation that only a dislocations slip transfer mechanism from the matrix to the hydride can explain. The plastic deformation of hydrides has been reported by many authors, either for solid hydrides [89,90,102] or as a secondary phase [47,52,53,81,100–110]. For example, some studies show that hydrides are able during loading to align themselves parallel to the applied stress before their fracture, which shows that they have a certain ability to deform [47,73,81].

TEM observations reveal a lot of possible interactions between dislocations or twins of the titanium or zirconium α-phase and the hydrides [44,52,53,104–107]. These interactions depend on the nature of the hydride, but also on the epitaxial orientation relationships between the

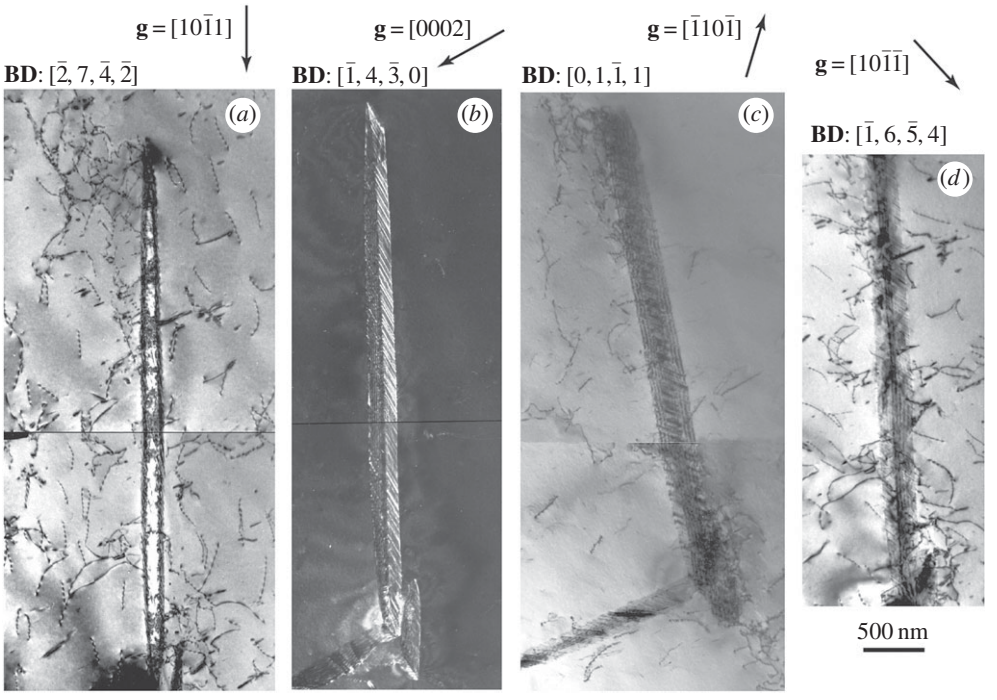

Figure 5. TEM identification of the interfacial dislocations on type II titanium γ-hydride after 1% plastic strain. (*a*) Beam direction: **BD**//($\bar{2}7\bar{4}2$) and **g** = (10$\bar{1}$1), BF. (*b*) **BD**//($\bar{1}4\bar{3}2$) and **g** = (0002), weak beam of hydride. (*c*) **BD**//(01$\bar{1}$1) and **g** = ($\bar{1}$10$\bar{1}$), BF. (*b*) **BD**//($\bar{1}6\bar{5}4$) and **g** = (10$\bar{1}\bar{1}$), BF.

Table 3. Characteristics of the dislocations present in the matrix and in the titanium/type II γ-hydride interface after 1% plastic strain identified from figure 5.

	OR II	$(0002)_{Ti}$// $(1\bar{1}\bar{1})_{\gamma}$ $[11\bar{2}0]_{Ti}$//$[110]_{\gamma}$
	habit plane	$(\bar{2}205)$
	matrix dislocations	$\vec{u} = [11\bar{2}0]$ $\vec{b} = \pm 1/3[\bar{1}\bar{1}20]$ $(\bar{1}100)$
	α-Ti interface dislocations	$\vec{u} = [11\bar{2}0]$ $\vec{b} = \pm 1/3[\bar{1}\bar{2}13]$ $(\bar{1}101)$
		$\vec{u} = [11\bar{2}0]$ $\vec{b} = \pm[0001]$ $(1\bar{1}00)$?
	γ-TiH interface dislocations	$\vec{u} = [110]$ $\vec{b} = \pm 1/2[101]$ $(1\bar{1}\bar{1})$
		$\vec{u} = [110]$ $\vec{b} = \pm 1/2[011]$ $(1\bar{1}1)$

α-phase and the hydride as well as the level of plastic strain. The most detailed studies concern titanium alloys whose texture is favourably oriented to prismatic slip [52,104–107]. Generally, the transfer of the deformation in the hydride does not depend on the type of hydride (γ or δ) but rather on the nature of the type I (OR1) and type II (OR2) epitaxial orientation relationships. This transfer can be the hydride shearing which classically occurs for small precipitates or the local destruction of the hydride (dissolution) favoured by a conjugate effect of temperature, stress and slip bands as well as by the intersection with a twin.

For type I hydrides (OR1), the presence of $\langle a \rangle$ dislocation at the hydride/matrix interface in the form of a pile [103] or not [104–107] leads to a more or less marked interface distortion (wavy character of the interface). This situation illustrates the presence of a high stress concentration,

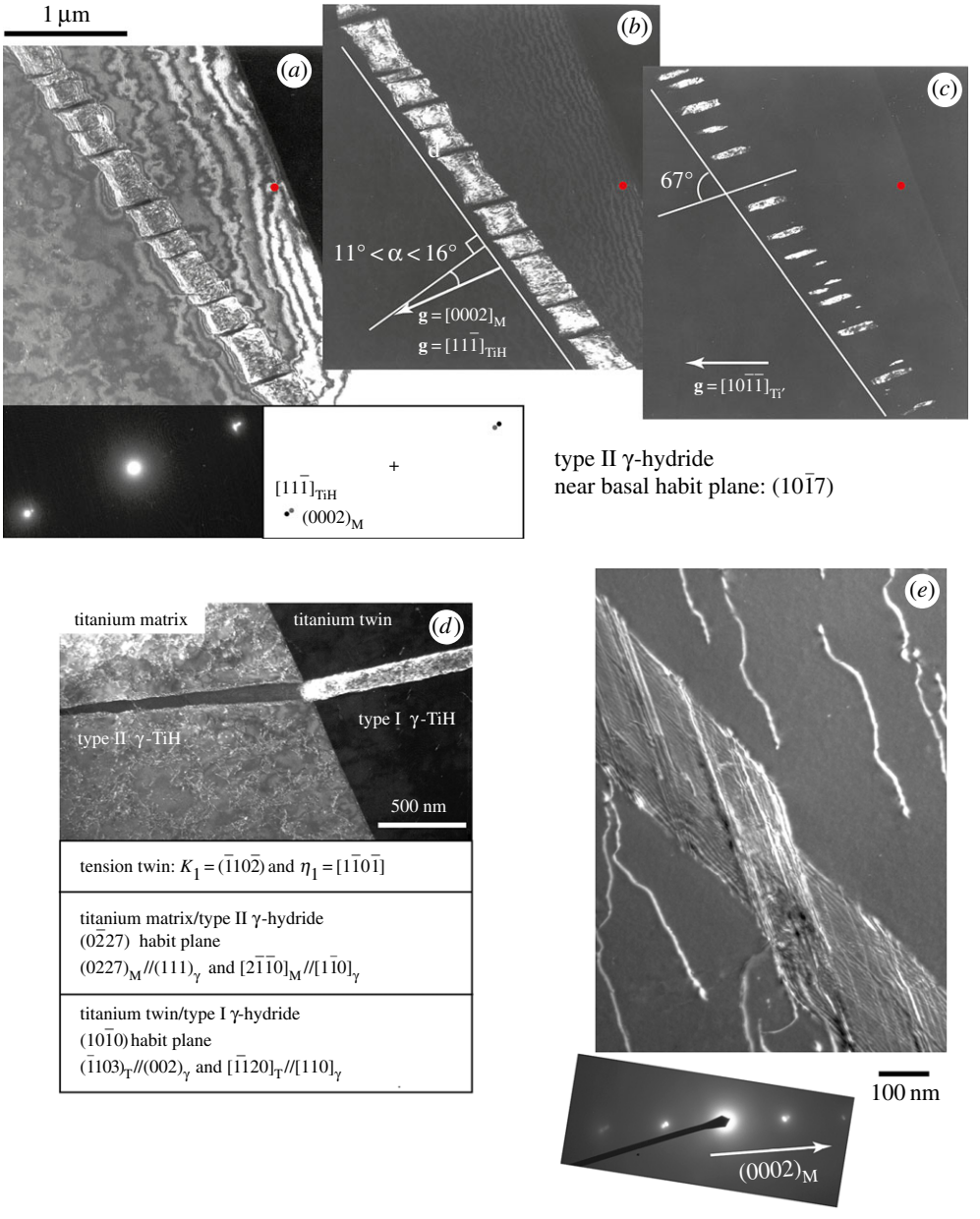

Figure 6. TEM observations at $\varepsilon_p = 6{\cdot}5\%$. (*a*) Weak beam of the titanium matrix, $\mathbf{g} = (0002)$. (*b*) Same area, dark field of the γ-hydride, $\mathbf{g} = (11\bar{1})$. (*c*) Same area, dark field of the titanium platelets, $\mathbf{g} = (10\bar{1}\bar{1})$. (*d*) Intersection of type II γ-hydride with a twin. (*e*) Shear of a type II γ-hydride by $\langle c + a \rangle$ dislocations, weak beam, $\mathbf{g} = (0002)$. (Online version in colour.)

which favours slip transmission when the hydrides are thin (thickness less than 400 nm). When the thickness of the hydrides increases the transfer of the slip is made more difficult, the hydride shear is less and the damage of the latter appears for a weaker deformation [104–107]. The Burgers vector of the dislocations observed in the γ- and δ-hydrides, as inclusions in the α-phase, is of type $1/2\langle 110 \rangle$ [104–107], which is in agreement with observations on polycrystalline solid hydrides [102]. The coherence of the interface between the hydrides of type I and the α-phase leads to a transfer of the deformation according to the following relation:

$$1/3\langle 11\bar{2}0 \rangle \rightarrow 1/2\langle 1\bar{1}0 \rangle + \vec{b}_r, \tag{4.2}$$

where $\overrightarrow{b}_r$ is a residual partial dislocation that can be described by a step left on the interface [104]. As this reaction is not energetically favourable, it can only occur under a stress concentration. Moreover, as the slip planes in the hydride are {111} type, the transmission of the slip requires a deviation process at the interface of the prismatic plane to the pyramidal plane π_1.

For type II hydrides (OR2), the angle between a prismatic plane and a {111} plane of the hydride is about 30°: the transfer of the deformation of the matrix to the hydride is also more difficult. On the other hand, for higher deformation rates, the activation of the basal and π_1 slips makes this transfer more favourable because of their better coincidence with the slip planes of the hydride. Thus, the TEM observations of figure 5 make it possible to identify in table 3 the dislocations formed at the interface between titanium matrix and type II γ-hydrides after a plastic strain in tension of 1%. The results seem to agree with the activation of the $\langle c+a\rangle$ pyramidal (π_1) slip in the matrix and $1/2\langle 1\bar{1}0\rangle\{111\}$ in the hydride but do not make it possible for now to understand the transmission of the sliding of the matrix to the hydride.

TEM observations performed at 6.5% plastic strain, prior to damage, resulted in the formation of special structures as shown in figure 6. For example, figure 6*a* shows a weak beam of a type II hydride under a basal diffraction vector of the matrix, whereas figure 6*b* corresponds to a dark field of the same hydride ($g=[11\bar{1}]$) with a near basal habit plane ($10\bar{1}7$). However, these two photographs show that the hydride has a 'palm tree trunk' appearance, each section separated from the others by platelets of a few tens of nanometres, which does not belong to the titanium matrix nor to the hydride. These platelets, which can be imaged in a dark field, cannot be indexed as twins of the hydride and have been identified as titanium having a different orientation from that of the matrix but having a type I orientation relationship with the mother hydride (figure 6*c*). These zones are therefore incoherent with the matrix, which favours the appearance of a stress field along the hydride between the platelets and the creation of accommodation dislocations at the tip of these platelets. Similarly, at the same plastic strain, the intersection of a tensile twin ($K_1=(\bar{1}10\bar{2})$ and $\eta_1=[1\bar{1}0\bar{1}]$) with a type II γ-hydride causes a reorientation of the latter so that it is found with a type I orientation relationship with the twin zone (figure 6*d*). Finally, the micrograph of figure 6*e* shows the shear of a type II hydride by $\langle c+a\rangle$ dislocations. These various transformations occur by shearing and/or by phase or orientation change ($\gamma \rightarrow$ Ti or $\gamma_{II} \leftrightarrow \gamma_I$ ...) which involves the diffusion of the hydrogen under the effect of the local stress.

5. Conclusion

This paper reports the substantial efforts to establish the impact of hydrogen on the viscoplastic and hardening behaviour of Ti-α and Zr-α alloys. Owing to low hydrogen solubility at room temperature, the real impact of the solute on the fundamental plasticity processes was improved only at temperatures higher than 500 K and depends mainly on oxygen content. Using a locking–unlocking model to describe the screw dislocation mobility, the consequences of hydrogen and oxygen contents on thermal-activated processes have been discussed. Some possible impacts of both solutes on dislocation core structure have been suggested. For larger hydrogen contents and lower temperatures, the kinetics of precipitation and dissolution of hydrides are partially clarified. The crystallographic coherence between the hexagonal substrate and the hydride precipitates is fairly high with particular epitaxial ORs. The thermal cyclic loading induces a deepening of misfit dislocations, which lead to the re-precipitation of hydrogen-poor hydride phases. The possible relationship between ORs and this process needs to be explored further.

The different interactions of the dislocations with the hydrides and their consequences on the strain hardening of Ti-α and Zr-α alloys were illustrated. It was clearly demonstrated the possible accommodation of the plastic strain by the hydrides and the partially reduction of the deformation incompatibilities between the hexagonal phase and hydride phases. This last point needs to be improved in relation with the different epitaxial orientation relationships.

Competing interests. We declare we have no competing interests.
Funding. No funding has been received for this article.

References

1. Domizzi G, Luppo MI, Vigna G. 2006 Microstructural features of the hydrogenation process in Ti grade 2. *J. Alloys Compd.* **424**, 193–198. (doi:10.1016/j.jallcom.2005.09.093)
2. Conforto E, Aronsson B-O, Salito A, Crestou C, Caillard D. 2004 Rough surfaces of titanium and titanium alloys for implants and prostheses. *Mater. Sci. Eng. C* **24**, 611–618. (doi:10.1016/j.msec.2004.08.004)
3. Lustmann B, Kerze F. 1955 *The metallurgy of zirconium*. New York, NY: McGraw-Hill.
4. Puls MP. 2012 *The effect of hydrogen and hydrides on the integrity of zirconium alloy components*. London, UK: Springer.
5. Conrad H. 1981 Effect of interstitial solutes on the strength and ductility of titanium. *Prog. Mater. Sci.* **26**, 123–403. (doi:10.1016/0079-6425(81)90001-3)
6. Barkia B, Doquet V, Couzinié JP, Guillot I, Héripré E. 2015 In situ monitoring of the deformation mechanisms in titanium with different oxygen content. *Mater. Sci. Eng. A* **636**, 91–102. (doi:10.1016/j.msea.2015.03.044)
7. Rautenberg M, Feaugas X, Poquillon D, Cloué JM. 2012 Microstructural characterization of creep anisotropy at 673 K in the M5 (R) alloy. *Acta Mater.* **60**, 4319–4327. (doi:10.1016/j.actamat.2012.04.001)
8. Khoda-Bakhsh R, Ross DK. 1982 Determination of the hydrogen site occupation in the α phase of zirconium hydride and in the α and β phases of titanium hydride by inelastic neutron scattering. *J. Phys. F: Metall. Phys.* **12**, 15–24. (doi:10.1088/0305-4608/12/1/003)
9. Domain C, Besson R, Legris A. 2002 Atomic-scale ab-initio study of the Zr-H system: I. Bulk properties. *Acta Mater.* **50**, 3513–3526. (doi:10.1016/S1359-6454(02)00173-8)
10. Mueller WM, Blackledge JP, Libowitz GC. 1968 *Metal hydrides*. New York, NY: Academic Press.
11. Conforto E, Cohendoz S, Berziou C, Girault P, Feaugas X. 2017 Formation and dissolution of hydride precipitates in zirconium alloys: crystallographic orientation relationships and stability after temperature cycling. *Mater. Sci. Forum* **879**, 2330–2335. (doi:10.4028/www.scientific.net/MSF.879.2330)
12. Feaugas X. 1994 Microstructure et modélisation du comportement en fatigue uniaxiale et multiaxiale d'un alliage de titane biphasé. PhD dissertation, Université de Technologie de Compiègne, France.
13. Geyer P. 1999 Comportement élasto-viscoplastique de tubes en zircaloy 4 : approche expérimentale et modélisation micromécanique. PhD dissertation, l'Ecole Nationale Supérieure des Mines de Paris, France.
14. Feaugas X, Conforto E. 2009 *PlastOx*2007, Argeles sur Mer, France, EDP Sciences, pp. 161–178.
15. Naka S, Lasalmonie A, Costa P, Kubin LP. 1988 The low-temperature plastic deformation of α-titanium and the core structure of a-type screw dislocations. *Phil. Mag. A* **57**, 717–740. (doi:10.1080/01418618808209916)
16. Farenc S, Caillard D, Couret A. 1993 An in situ study of prismatic glide in α titanium at low temperatures. *Acta Metall. Mater.* **41**, 2701–2709. (doi:10.1016/0956-7151(93)90139-J)
17. De Crecy A, Bourret A, Naka S, Lasalmonie A. 1983 High resolution determination of the core structure of 1/3 ⟨1120⟩ {1010} edge dislocation in titanium. *Phil. Mag. A* **47**, 245–254. (doi:10.1080/01418618308245221)
18. Legrand B. 1984 Structure du coeur des dislocations vis. 1/3⟨1120⟩ dans le titane. *Phil. Mag. A* **52**, 83–97. (doi:10.1080/01418618508237608)
19. Viteck V. 1974 Theory of core structures of dislocations in body-centered cubic metals. *Cryst. Lattice Defects* **5**, 1–34.
20. Ferrer F. 1999 Etude des mécanismes de déformation du zirconium entre 25°C et 400°C. Influence d'une faible teneur en soufre. PhD dissertation, Ecole Polytechnique, France.
21. Clouet E. 2012 Screw dislocation in zirconium: an ab initio study. *Phys. Rev. B* **86**, 144104. (doi:10.1103/PhysRevB.86.144104)
22. Rodney D, Ventelon L, Clouet E, Pizzagalli L, Willaime F. 2017 Ab initio modeling of dislocation core properties in metals and semiconductors. *Acta Mater.* **124**, 633–659. (doi:10.1016/j.actamat.2016.09.049)

23. Paton NE, Backofen WA. 1970 Plastic deformation of titanium at elevated temperatures. *Metall. Trans. A* **1**, 2839–2847. (doi:10.1007/BF03037822)
24. Pelissie C, Guetaz L, Baillin X, Moret F. 1996 Deformation modes of Ti-6Al-4V at cryogenic temperatures. *Revue de Metallurgie: Cahiers d'Informations Techniques* **93**, 1509.
25. Churchman AT. 1954 The slip modes of titanium and the effect of purity on their occurrence during tensile deformation of single crystals. *Proc. R. Soc. A* **226**, 216–226. (doi:10.1098/rspa.1954.0250)
26. Levine ED. 1966 Deformation mechanisms in titanium at low temperatures. *Trans. Met. Soc. AIME* **236**, 1558–1565.
27. Williams JC, Sommer AW, Tung PP. 1968 The influence of oxygen concentration on the internal stress and dislocation arrangements in α titanium. *Metall. Trans. A* **3**, 2979–2984. (doi:10.1007/BF02652870)
28. Aktar A. 1975 Basal slip and twinning in α-titanium single crystals. *Metall. Trans. A* **6**, 1105–1113. (doi:10.1007/BF02661366)
29. Paton NE, Williams JC, Rauscher GP. 1973 The deformation of α-phase titanium. In *Titanium science and technology* (eds RI Jaffe, HM Burte), pp. 1049–1069. New York, NY: Plenum Press.
30. Jones IP, Hutchinson WB. 1981 Stress-state dependence of slip in titanium-6Al-4 V and other HCP metals. *Acta. Metall.* **29**, 951–968. (doi:10.1016/0001-6160(81)90049-3)
31. Chan KS, Wojcik CC, Koss A. 1981 Deformation of an alloy with a lamellar microstructure: experimental behavior of individual widmanstatten colonies of an α-β titanium alloy. *Metall. Trans. A* **12**, 1899–1907. (doi:10.1007/BF02643801)
32. Lecomte JS, Philippe MJ, Klimanek P. 1987 Plastic deformation of a Ti-6% Al-4% V alloy with a strong transverse-type crystallographic α-texture at elevated temperatures. *Mater. Sci. Eng. A* **A234**, 869–872. (doi:10.1016/S0921-5093(97)00416-4)
33. Bridier F, Villechaise P, Mendez J. 2005 Analysis of the different slip systems activated by tension in a α/β titanium alloy in relation with local crystallographic orientation. *Acta Mater.* **53**, 555–567. (doi:10.1016/j.actamat.2004.09.040)
34. Aktar A. 1973 Compression of zirconium single crystals parallel to the c-axis. *J. Nucl. Mater.* **47**, 79–86. (doi:10.1016/0022-3115(73)90189-X)
35. Bacon DJ, Liang MH. 1986 Computer simulation of dislocation cores in h.c.p. metals I. Interatomic potentials and stacking-fault stability. *Phil. Mag. A* **53**, 163–179. (doi:10.1080/01418618608242819)
36. Liang MH, Bacon DJ. 1986 Computer simulation of dislocation cores in h.c.p. metals II. Core structure in unstressed crystals. *Phil. Mag. A* **53**, 180–204. (doi:10.1080/01418618608242820)
37. Liang MH, Bacon DJ. 1986 Computer simulation of dislocation cores in h.c.p. metals III. The effect of applied shear strain. *Phil. Mag. A* **53**, 205–220. (doi:10.1080/01418618608242821)
38. Minonishi Y, Morozumi S. 1982 {1122} ⟨1123⟩ slip in titanium. *Scr. Metall.* **16**, 427–430. (doi:10.1016/0036-9748(82)90166-1)
39. Numakura H, Minonishi Y, Koiwa M. 1986 ⟨1123⟩ {1011} slip in titanium polycrystals at room temperature. *Scr. Metall.* **20**, 1581–1586. (doi:10.1016/0036-9748(86)90399-6)
40. Numakura H, Minonishi Y, Koiwa M. 1991 ⟨1123⟩ {1011} slip in zirconium. *Phil. Mag. A* **63**, 1077–1084. (doi:10.1080/01418619108213938)
41. Farenc S, Caillard D, Couret A. 1995 A new model for the peak of activation area of α titanium. *Acta Metall. Mater.* **43**. 3669–3678. (doi:10.1016/0956-7151(95)90150-7)
42. Caillard D, Martin JL. 2003 *Thermally activated mechanisms in crystal plasticity*. Amsterdam, The Netherlands: Elsevier Science.
43. Feaugas X. In press. On the impact of oxygen and hydrogen on the deformation of α-phase zirconium. *Phys. Stat. Sol. A*.
44. Rupa N. 2000 Effet de l'hydrogène et des hydrures sur le comportement viscoplastique du zircaloy-4 recristallisé. PhD dissertation, Université de Technologie de Compiègne, France. See http://www.iaea.org/inis/collection/NCLCollectionStore/_Public/38/105/38105101.pdf.
45. Barkia B, Doquet V, Couzinié JP, Guillot I. 2015 Room-temperature creep and stress relaxation in commercial purity titanium—influence of the oxygen and hydrogen contents on incubation phenomena and aging-induced rejuvenation of the creep potential. *Mater. Sci. Eng. A* **A624**, 79–89. (doi:10.1016/j.msea.2014.11.073)

46. Domain C, Besson R, Legris A. 2004 Atomic-scale ab initio study of the Zr–H system. II. Interaction of H with plane defects and mechanical properties. *Acta Mater.* **52**, 1495–1502. (doi:10.1016/j.actamat.2003.11.031)
47. Bai J, Ji N, Gilbon D, Prioul C, François D. 1994 Hydride embrittlement in ZIRCALOY-4 plate. Part II. Interaction between the tensile stress and the hydride morphology. *Metall. Mater. Trans. A* **25**, 1199–1208. (doi:10.1007/BF02652294)
48. Sofronis P, Birnbaum HK. 1995 Mechanics of the hydrogen–dislocation–impurity interactions. I. Increasing shear modulus. *J. Mech. Phys. Solids* **43**, 49–90. (doi:10.1016/0022-5096(94)00056-B)
49. Chateau JP, Delafosse D, Magnin T. 2002 Numerical simulations of hydrogen–dislocation interactions in fcc stainless steels: part I: hydrogen–dislocation interactions in bulk crystals. *Acta Mater.* **6**, 1507–1522. (doi:10.1016/S1359-6454(02)00008-3)
50. Chateau JP, Delafosse D, Magnin T. 2002 Numerical simulations of hydrogen–dislocation interactions in fcc stainless steels: part II: hydrogen effects on crack tip plasticity at a stress corrosion crack. *Acta Mater.* **6**, 1507–1522. (doi:10.1016/S1359-6454(02)00009-5)
51. Shih DS, Robertson IM. 1988 Hydrogen embrittlement of α titanium: in situ TEM studies. *Acta Metall.* **36**, 111–124. (doi:10.1016/0001-6160(88)90032-6)
52. Guillot I, Feaugas X, Clavel M. 2001 Dislocation-hydride interactions at low plastic strain in titanium. *Scr. Mater.* **44**, 1011–1017. (doi:10.1016/S1359-6462(01)00672-8)
53. Huez J, Feaugas X, Helber AL, Guillot I, Clavel M. 1998 Damage process in commercially pure α-titanium alloy without (Ti40) and with (Ti40-H) hydrides. *Metall. Trans. A* **29**, 1615–1628. (doi:10.1007/s11661-998-0085-2)
54. Perovic V, Weatherly GC, MacEwen SR, Leger M. 1992 The influence of prior deformation on hydride precipitation in zircaloy. *Acta Metall.* **40**, 363–372. (doi:10.1016/0956-7151(92)90310-B)
55. Luppo MI, Politi A, Vigna G. 2005 Hydrides in α-Ti: characterization and effect of applied external stresses. *Acta Mater.* **53**, 4987–4996. (doi:10.1016/j.actamat.2005.06.004)
56. Conforto E, Caillard D. 2007 A fast method for determining favourable orientation relationships and interface planes: application to titanium–titanium hydrides transformations. *Acta Mater.* **55**, 785–798. (doi:10.1016/j.actamat.2006.06.061)
57. Moore KE, Young WA. 1968 Phase studies of the Zr-H systems at high hydrogen concentrations. *J. Nucl. Mater.* **27**, 316–324. (doi:10.1016/0022-3115(68)90090-1)
58. Barraclough KG, Beevers CJ. 1970 Some observations on the phase transformations in zirconium hydrides. *J. Nucl. Mater.* **34**, 125–134. (doi:10.1016/0022-3115(70)90112-1)
59. Irving PE, Beevers CJ. 1971 Some metallurgical and lattice parameter observations on titanium hydride. *Metall. Trans. A* **2**, 613–615. (doi:10.1007/BF02663362)
60. Bradbrook JS, Lorimer GW, Ridley N. 1972 The precipitation of zirconium hydride in zirconium and zircalloy-2. *J. Nucl. Mater.* **42**, 142–160. (doi:10.1016/0022-3115(72)90021-9)
61. Carpenter GJC, Watters JF, Gilbert RW. 1973 Dislocations generated by zirconium hydride precipitates in zirconium and some of its alloys. *J. Nucl. Mater.* **48**, 267–276. (doi:10.1016/0022-3115(73)90023-8)
62. Carpenter GJC. 1978 The precipitation of γ-zirconium hydride in zirconium. *Acta Metall.* **26**, 1225–1235. (doi:10.1016/0001-6160(78)90006-8)
63. Weatherly GC. 1981 The precipitation of γ-hydride plates in zirconium. *Acta Metall.* **29**, 501–512. (doi:10.1016/0001-6160(81)90074-2)
64. Numakura H, Koiwa M. 1984 Hydride precipitation in titanium. *Acta Metall.* **32**, 1799–1807. (doi:10.1016/0001-6160(84)90236-0)
65. Woo OT, Weatherly GC, Coleman CE, Gilbert RW. 1985 The precipitation of γ-deuterides (hydrides) in titanium. *Acta Metall.* **33**, 1897–1906. (doi:10.1016/0001-6160(85)90011-2)
66. Woo OT, Carpenter GJC. 1985 γ-TiH: an isomorph of γ-ZrH. *Scr. Metall.* **19**, 931–934. (doi:10.1016/0036-9748(85)90285-6)
67. Puls MP. 1984 Elastic and plastic accommodation effects on metal-hydride solubility. *Acta Metall.* **32**, 1259–1269. (doi: 10.1016/0001-6160(84)90133-0)
68. Zhang CB, Kang Q, Lai ZH, Ji R. 1996 The microstructural modification, lattice defects and mechanical properties of hydrogenated/dehydrogenated α-Ti. *Acta Metall. Mater.* **44**, 1077–1084. (doi: 0956-7151(95)00211-1)

69. Aladjem A. 1996 Zirconium-hydrogen. *Solid State Phen.* **49–50**, 281–329. (doi:10.4028/www.scientific.net/SSP.49-50.281)
70. Manchester FD. 2000 *Phase diagrams of binary hydrogen alloys*, p. 238. Materials Park, OH: ASM International.
71. Wu TI, Wu JK. 2002 Effects of electrolytic hydrogenating parameters on structure and composition of surface hydrides of CP-Ti and Ti–6Al–4 V alloy. *Mater. Chem. Phys.* **74**, 5–12. (doi:10.1016/S0254-0584(01)00403-5)
72. Conforto E, Feaugas X. 2015 Hydrides formation and dissolution processes in zirconium alloys: crystallographic orientation relationships and stability after temperature cycling. *Proc. PTM* **2015**, 231–238.
73. Bai J, Prioul C, François D. 1994 Hydride embrittlement in ZIRCALOY-4 plate: part I. Influence of microstructure on the hydride embrittlement in ZIRCALOY-4 at 20°C and 350°C. *Metall. Mater. Trans. A* **25**, 1185–1197. (doi:10.1007/BF02652293)
74. Cann CD, Puls MP, Sexton EE, Hutchings WG. 1984 The effect of metallurgical factors on hydride phases in zirconium. *J. Nucl. Mater.* **126**, 197–205. (doi:10.1016/0022-3115(84)90029-1)
75. Root JH, Small WM, Khatamian D, Woo OT. 2003 Kinetics of the δ to γ zirconium hydride transformation in Zr-2.5Nb. *Acta Mater.* **51**, 2041–2053. (doi:10.1016/S1359-6454(03)00004-1)
76. Zuzek E. 1990 H-Zr binary alloy phase diagram. In *Binary alloy phase diagrams*, 2nd edn (eds TB Massalski, H Okamoto, PR Subramanian, L Kacprzak), p. 2070. Materials Park, OH: ASM International.
77. Northwood DO, Kosasih U. 1983 Hydrides and delayed hydrogen cracking in zirconium and its alloys. *Int. Met. Rev.* **28**, 92–121. (doi:10.1179/imtr.1983.28.1.92)
78. Bourret A, Lasalmonie A, Naka S. 1986 In-situ high resolution observation of hydride precipitation in titanium. *Scr. Metall.* **20**, 861–866. (doi:10.1016/0036-9748(86)90455-2)
79. Conforto E, Caillard D. 2011 Edge-to-edge matching at Ti-TiH interfaces: kinetics of hydride growth and clustering of precipitates with different orientation relationships. *Solid State Phenomena* **172–174**, 242–247. (doi:10.4028/www.scientific.net/SSP.172-174.242)
80. Kim J-S, Kim S-D, Yoon J. 2016 Hydride formation on deformation twin in zirconium alloy. *J. Nucl. Mater.* **482**, 88–92. (doi:10.1016/j.jnucmat.2016.10.020)
81. Vicente Alvarez MA, Santisteban JR, Vizcaíno P, Ribarik G, Ungar T. 2016 Quantification of dislocations densities in zirconium hydride by X-ray line profile analysis. *Acta Mater.* **117**, 1–12. (doi:10.1016/j.actamat.2016.06.058)
82. Fukai Y. 2005 *The metal-hydrogen system: basic bulk properties*. New York, NY: Springer.
83. Une K, Ishimoto S. 2003 Dissolution and precipitation behavior of hydrides in Zircaloy-2 and high Fe Zircaloy. *J. Nucl. Mater.* **322**, 66–72. (doi:10.1016/S0022-3115(03)00320-9)
84. Tang R, Yang X. 2015 Dissolution and precipitation behaviors of hydrides in N18, Zry-4 and M5 alloys. *Int. J. Hyd. Energy* **34**, 7269–7274. (doi:10.1016/j.ijhydene.2009.07.018)
85. Vizcaino P, Rios RO, Banchik AD. 2005 Hydrogen determinations in a zirconium based alloy with a DSC. *Thermochim. Acta* **429**, 7–11. (doi:10.1016/j.tca.2004.11.019)
86. Conforto E, Cohendoz S, Girault P, Berziou C, Feaugas X. 2017 Hydride precipitates in zirconium alloys. In *TMS2017: 146th Annual Meeting & Exhibition supplemental proceedings*, pp. 771–782. Cham, Switzerland: Springer International. (doi:10.1007/978-3-319-51493-2_74)
87. Choubey R, Puls MP. 1994 Crack initiation at long radial hydrides in Zr-2.5Nb pressure tube material at elevated temperatures. *Metall. Mater. Trans. A* **25**, 993–1004. (doi:10.1007/BF02652274)
88. Chan KS. 1995 A fracture model for hydride-induced embrittlement. *Acta Metall. Mater.* **43**, 4325–4335. (doi:10.1016/0956-7151(95)00133-G)
89. Barraclough KG, Beevers CJ. 1969 Some observations on the deformation characteristics of bulk polycrystalline zirconium hydrides. Part 1: the deformation and fracture of hydrides based on the δ-phase. *J. Mater. Sci.* **4**, 518–525. (doi:10.1007/BF00550212)
90. Beevers CJ, Barraclough KG. 1969 Some observations on the deformation characteristics of bulk polycrystalline zirconium hydrides. Part 2: the deformation of ε-hydrides. *J. Mater. Sci.* **4**, 802–808. (doi:10.1007/BF00551076)
91. Puls MP, Shi J, Rabier SQ. 2005 Experimental studies of mechanical properties of solid zirconium hydrides. *J. Nucl. Mater.* **336**, 73–80. (doi:10.1016/j.jnucmat.2004.08.016)

92. Xu JJ, Cheung HY, Shi SQ. 2007 Mechanical properties of titanium hydride. *J. Alloys Compd.* **436**, 82–85. (doi:10.1016/j.jallcom.2006.06.107)
93. Lanin AG, Zalivin IM, Turchin VN, Boiko EB. 1984 Mechanical properties of zirconium, titanium, and yttrium hydride alloys. *Strength Mater.* **16**, 869–876. (doi:10.1007/BF01529980)
94. Yamanaka S, Yoshioka K, Uno M, Katsura M, Anada H, Matsuda T, Kobayashi S. 1999 Thermal and mechanical properties of zirconium hydride. *J. Alloys Compd.* **293–295**, 23–29. (doi:10.1016/S0925-8388(99)00389-8)
95. Xu JJ, Shi SQ. 2004 Investigation of mechanical properties of ε-zirconium hydride using micro- and nano-indentation techniques. *J. Nucl. Mater.* **327**, 165–170. (doi:10.1016/j.jnucmat.2004.02.004)
96. Kuroda M, Setoyama D, Uno M, Yamanaka S. 2004 Nanoindentation studies of zirconium hydride. *J. Alloys Compd.* **368**, 211–214. (doi:10.1016/j.jallcom.2003.08.094)
97. Rico A, Martin-Rengel MA, Ruiz-Hervias J, Rodriguez J, Gomez-Sanchez FJ. 2014 Nanoindentation measurements of the mechanical properties of zirconium matrix and hydrides in unirradiated pre-hydrided nuclear fuel cladding. *J. Nucl. Mater.* **452**, 69–76. (doi:10.1016/j.jnucmat.2014.04.045)
98. Nix WD, Gao H. 1998 Indentation size effects in crystalline materials: a law for strain gradient plasticity. *J. Mech. Phys. Solids* **46**, 411–425. (doi:10.1016/S0022-5096(97)00086-0)
99. Oono N *et al.* 2013 Comparison of irradiation hardening an microstructure evolution in ion-irradiated delta and epsilon hydrides. *J. Nucl. Mater.* **442**, S826–S829. (doi:10.1016/j.jnucmat.2013.03.013)
100. Setoyama D, Matsunaga J, Muta H, Uno M, Yamanaka S. 2004 Mechanical properties of titanium hydride. *J. Alloys Compd.* **381**, 215–220. (doi:10.1016/j.jallcom.2004.04.073)
101. Brown LM, Clarke DR. 1975 Work hardening due to internal stresses in composite materials. *Acta Metall.* **23**, 821–830. (doi:10.1016/0001-6160(75)90198-4)
102. Irving PE, Beevers CJ. 1972 Some observations on the deformation characteristics of titanium hydride. *J. Mater. Sci.* **7**, 23–30. (doi:10.1007/BF00549545)
103. Grange M, Besson J, Andrieu E. 2000 Anisotropic behavior and rupture of hydrided ZIRCALOY-4 sheets. *Metall. Mater. Trans. A* **31A**, 679–690. (doi:10.1007/s11661-000-0010-9)
104. Chen CQ, Li SX, Lu K. 2003 The deformation behaviors of gamma hydrides in titanium under cyclic straining. *Acta Mater.* **51**, 931–942. (doi:10.1016/S1359-6454(02)00495-0)
105. Chen CQ, Li SX, Lu K. 2004 Dislocation interaction with hydrides in titanium containing a low hydrogen concentration. *Philos. Mag.* **84**, 29–43. (doi:10.1080/14786430310001623533)
106. Chen CQ, Li SX. 2004 Tensile and low-fatigue behaviors of commercially pure titanium containing γ hydrides. *Mater. Sci. Eng. A* **387–389**, 470–475. (doi:10.1016/j.msea.2004.01.117)
107. Chen CQ, Li SX, Zheng H, Wang LB, Lu K. 2004 An investigation on structure, deformation and fracture of hydrides in titanium with a large range of hydrogen contents. *Acta Mater.* **52**, 3697–3706. (doi:10.1016/j.actamat.2004.04.024)
108. Veleva M, Arsen S, Record MC, Bechade JL, Bai J. 2003 Hydride embrittlement and irradiation effects on the hoop mechanical properties of pressurized water reactor (PWR) and boiling-water reactor (BWR) ZIRCALOY cladding tubes. Part II. Morphology of hydrides investigated at different magnifications and their interaction with the processes of plastic deformation. *Metall. Mater. Trans. A* **34**, 567–578. (doi:10.1007/s11661-003-0092-2)
109. Arsen S, Bai J, Bompard P. 2003 Hydride embrittlement and irradiation effects on the hoop mechanical properties of pressurized water reactor (PWR) and boiling-water reactor (BWR) ZIRCALOY cladding tubes. Part III. Mechanical behavior of hydride in stress-relived annealed and recrystallized ZIRCALOYs. *Metall. Mater. Trans. A* **34**, 579–588. (doi:10.1007/s11661-003-0093-1)
110. Weekes HE, Vorotsov VA, Dolbnya IP, Plummer JD, Giuliani F, Britton TB, Dye D. 2015 In situ micropillar deformation of hydrides in Zircaloys-4. *Acta Mater.* **92**, 81–96. (doi:10.1016/j.actamat.2015.03.037)